# Assessment of coronary microcirculation alterations in a porcine model of no-reflow using ultrasound localization microscopy: a proof of concept study

Oscar Demeulenaere, Philippe Mateo, René Ferrera, Paul-Mathieu Chiaroni, Alain Bizé, Jianping Dai, Lucien Sambin, Romain Gallet, Mickaël Tanter, Clément Papadacci, et al.

# Assessment of coronary microcirculation alterations in a porcine model of no-reflow using ultrasound localization microscopy: a proof of concept study

Oscar Demeulenaere,[a] Philippe Mateo,[a] René Ferrera,[b] Paul-Mathieu Chiaroni,[c,d] Alain Bizé,[c] Jianping Dai,[c] Lucien Sambin,[c] Romain Gallet,[c,d] Mickaël Tanter,[a] Clément Papadacci,[a,*] Bijan Ghaleh,[c] and Mathieu Pernot[a]

[a]Physics for Medicine, ESPCI, INSERM U1273, CNRS UMR 8063, PSL University, Paris, France
[b]CarMeN, 27102 INSERM U1060, INRA U1397, INSA de Lyon, Université Claude Bernard Lyon 1, Université de Lyon, Villeurbanne, France
[c]Inserm U955-IMRB, UPEC, Ecole Nationale Vétérinaire d'Alfort, F-94700, Créteil, France
[d]APHP, Hôpitaux Universitaires Henri Mondor, Service de Cardiologie, F-94000, Créteil, France

eBioMedicine
2023;94: 104727
Published Online 22 July 2023
https://doi.org/10.1016/j.ebiom.2023.104727

## Summary

**Background** Coronary microvascular obstruction also known as no-reflow phenomenon is a major issue during myocardial infarction that bears important prognostic implications. Alterations of the microvascular network remains however challenging to assess as there is no imaging modality in the clinics that can image directly the coronary microvascular vessels. Ultrasound Localization Microscopy (ULM) imaging was recently introduced to map microvascular flows at high spatial resolution (~10 µm). In this study, we developed an approach to image alterations of the microvascular coronary flow in *ex vivo* perfused swine hearts.

**Methods** A porcine model of myocardial ischemia-reperfusion was used to obtain microvascular coronary alterations and no-reflow. Four female hearts with myocardial infarction in addition to 6 controls were explanted and placed immediately in a dedicated preservation and perfusion box manufactured for ultrasound imaging. Microbubbles (MB) were injected into the vasculature to perform Ultrasound Localization Microscopy (ULM) imaging and a linear ultrasound probe mounted on a motorized device was used to scan the heart on multiple slices. The coronary microvascular anatomy and flow velocity was reconstructed using dedicated ULM algorithms and analyzed quantitatively.

**Findings** We were able to image the coronary microcirculation of *ex vivo* swine hearts at a resolution of tens of microns and measure flow velocities ranging from 10 mm/s in arterioles up to more than 200 mm/s in epicardial arteries. Under different aortic perfusion pressures, we measured in large arteries of a subset of control hearts an increase of flow velocity from 31 ± 11 mm/s at 87 mmHg to 47 ± 17 mm/s at 132 mmHg (N = 3 hearts, $P < 0.05$). This increase was compared with a control measurement with a flowmeter in the aorta. We also compared 6 control hearts to 4 hearts in which no-reflow was induced by the occlusion and reperfusion of a coronary artery. Using average MB velocity and average density of MB per unit of surface as two ULM quantitative markers of perfusion, we were able to detect areas of coronary no-reflow in good agreement with a control anatomical pathology analysis of the cardiac tissue. In the no-reflow zone, we measured an average perfusion of 204 ± 305 MB/mm$^2$ compared to 3182 ± 1302 MB/mm$^2$ in the surrounding re-perfused area.

**Interpretation** We demonstrated this approach can directly image and quantify coronary microvascular obstruction and no-reflow on large mammal perfused hearts. This is a first step for noninvasive, quantitative and affordable assessment of the coronary microcirculation function and particularly coronary microvascular anatomy in the infarcted heart. This approach has the potential to be extended to other clinical situations characterized by microvascular dysfunction.

*Abbreviations:* 2D, 2 dimensions; 3D, 3 dimensions; AHA, American Heart Association; CFR, Coronary flow reserve; CT, X-ray computed tomography; ECG, Electrocardiogram; FWHM, Full Width Half Maximum; GPU, Graphics processing unit; IQ, In-phase and quadrature; IQR, Interquartile range; LAD, Left anterior descending artery; LV, Left ventricle; MB, Microbubbles; MRI, Magnetic resonance imaging; NR, No-reflow; PET, Positron emission tomography; PRF, Pulse repetition frequency; PSF, Point spread function; RCA, Row-Column Addressed probe; RV, Right ventricle; SVD, Singular Value Decomposition; TTC, TriphenylTetrazolium chloride; ULM, Ultrasound Localization Microscopy; UV, Ultraviolet

*Corresponding author. Physics for Medicine, ESPCI, CNRS, PSL, PariSante Campus, 2-10 rue d'Oradour-sur-Glane, 75015, Paris, France.
*E-mail address:* clement.papadacci@espci.fr (C. Papadacci).

Funding This study was supported by the French National Research Agency (ANR) under ANR-21-CE19-0002 grant agreement.



Keywords: Coronary microcirculation; No-reflow; Medical imaging; Ultrasound; ULM

### Research in context

#### Evidence before this study

Rapid and complete reperfusion of occluded coronary artery is essential in managing myocardial infarction. No-reflow is a phenomenon where proper downstream myocardial reperfusion fails despite opening the culprit coronary artery. No-reflow involves multiple factors such as leaky vessels, dysfunctional microvessels, embolization, and vascular compression due to edema. It is predictive of poor clinical outcomes, adverse left ventricular remodeling, and heart failure. Thus its diagnosis is crucial in managing myocardial infarction.

Conventional imaging tools lack sufficient spatial resolution to directly observe microvascular vessels (<100 μm) in the coronary circulation. As a result, functional assessment at the macroscopic level using techniques like PET, MRI, and contrast echocardiography is used to indirectly investigate the coronary microcirculation. These examinations provide information on hemodynamics, such as myocardial blood flow and coronary flow reserve (CFR). However, direct imaging of the coronary microcirculation in clinical settings is currently not possible with existing imaging modalities. Ultrasound Localization Microscopy (ULM) imaging enables high spatial resolution (~10 μm) mapping of microvascular flows, surpassing the traditional diffraction limit and imaging depth. A recent 3D approach using ULM with ultrafast ultrasound imaging successfully imaged the entire coronary microvasculature in rat hearts *ex vivo* and *in vivo*. However current systems have limited field of view for large mammal hearts.

#### Added value of this study

The study aimed to assess the use of ULM for investigating alterations in the coronary microcirculation in large porcine hearts. A new and simple approach was developed to image entirely the coronary microcirculation in *ex vivo* perfused hearts at a resolution of tens of microns (~25 μm). The approach was validated in a pig model of myocardial infarction and no-reflow, comparing hearts with normal function (N = 6) to those with altered microcirculation (N = 4).

#### Implications of all the available evidence

The study presents an approach for studying coronary microcirculation and no-reflow in large animal preclinical models, such as swine. The designed experimental setup is rapid and simple and is the only imaging modality that can map the coronary flows in a large heart at a microscopic scale. It has the potential to be a promising solution for studying coronary perfusion and no-reflow of the reperfused heart in the acute phase of myocardial infarction. The approach could be extended to the diagnosis of coronary microvascular dysfunction in other clinical situations.

## Introduction

Rapid and complete reperfusion of the occluded coronary artery is the corner stone of the current management of myocardial infarction. However, although the culprit epicardial coronary artery is fully opened with angioplasty or thrombolysis, numerous patients fail to present proper downstream myocardial reperfusion due to altered microvascular coronary circulation, a phenomenon so-called no-reflow.[1] The no-reflow is multifactorial and encompasses interacting processes such as leaky vessels, dysfunctional microvessels, distal embolization or vascular compression due to edema. The no-reflow phenomenon is predictive of poor clinical outcome and higher prevalence of post-myocardial infarction complications, adverse left ventricular remodeling and heart failure.[2] Therefore, its diagnosis remains an important goal to achieve.

Although conventional imaging tools can assess directly the anatomy of large coronary vessels, their spatial resolution is not sufficient to observe directly the microvascular vessels (<100 μm). As a consequence, the coronary microcirculation is currently investigated indirectly by functional assessment at the macroscopic level using positron emission tomography (PET),[3] cardiac magnetic resonance imaging (MRI),[4] contrast echocardiography[5] or through invasive measurements.[6] These examinations can reveal hemodynamic information such as myocardial blood flow and coronary flow reserve (CFR). However, direct imaging of the coronary microcirculation in clinical settings is still not possible with current imaging modalities, which has significantly hampered our understanding of the pathophysiology of the coronary microcirculation.

Ultrasound Localization Microscopy (ULM) imaging was recently introduced to map microvascular flows at high spatial resolution (~10 µm), an order of magnitude smaller than the ultrasonic diffraction limit, and at depths far greater than the traditionally frequency-limited imaging depth.[7–9] In,[10] imaging of the rat coronary microcirculation was performed in 2D with ULM. We recently developed a 3D approach based on ULM with ultrafast ultrasound imaging to image the entire coronary microvasculature in beating rat hearts *ex vivo* and *in vivo*.[11] Yet a high frequency matrix array probe with a limited field of view compared to the size of a human heart was used in this proof of concept. Today, there is no system available to image large mammal hearts.

The objective of this study was to investigate whether ULM can assess alterations of the coronary microcirculation in *ex vivo* perfused porcine hearts as a first proof of concept. We developed a new and simple approach adapted to image the coronary microcirculation of large *ex vivo* hearts. We validated this approach in a pig model of myocardial infarction and subsequent no-reflow (N = 4) compared to normal hearts (N = 6).

## Methods

### Model of no-reflow

Ten female Landrace Large-White crossed swine (27 ± 1 kg) hearts were evaluated. Control hearts (N = 6) were harvested under normal conditions in the absence of myocardial ischemia-reperfusion. Pigs were sedated with a mixture of zolazepam-tiletamine (both 10 mg/kg) received pentobarbital (50 mg/kg) before harvesting the heart under left thoracotomy. In the no-reflow (NR) group, under fluoroscopic guidance and anesthesia (isoflurane 1–2%), four pigs underwent an episode of 60 min of ischemia induced by the inflation of an angioplasty balloon in the left anterior descending coronary artery (LAD), followed by its deflation to allow reperfusion during 4 days.

### Experimental setup: isolated perfused non-beating heart

Under anesthesia and during euthanasia, the heart was harvested, cannulated at the level of the ascending aorta, and perfused in the reverse direction, according to the Langendorff method with oxygenated Krebs-Henseleit solution maintained at 4 °C and a perfusion rate at approximately 0.2 L/min. To perform ultrasound imaging a dedicated preservation box minimizing the absorption and the reflection of ultrasound energy was manufactured. This preservation container has a hexagonal shape. Each facet enables longitudinal and transversal scans of the heart allowing a full exploration. The whole box was manufactured by Goodfellow (Lille, France) using a TPX polymer, material used for his its low acoustic attenuation and low acoustic impedance mismatch.[12] The *ex vivo* heart was placed within this box filled with Krebs-Henseleit solution. Cardiac arrest was achieved by lowering the temperature of the solution from 37 °C to 4 °C. A 5 mL microbubbles (MB) solution (SonoVue®, Bracco) was added to the infusion perfusion flow of 0.2 mL/min with a syringe pump with a concentration of 100% and a flow rate of 15 mL/h (Fig. 1) corresponding to a 800:1 dilution of the initial Sonovue solution.

The circulation was done as follow: the Krebs-Henseleit solution is placed high up to perfuse the aorta via a cannula. The solution perfuses the coronary arteries, exits through the venous network and the coronary sinus, flows into the right atrium and then into the right ventricle to exit through the pulmonary artery (which is severed) and contributes to filling the box. The solution is then pumped at the base of the box by a peristaltic pump to the container filled with Krebs-Henseleit located above. The pressure difference between the overhead container and the heart will allow perfusion to the aorta to complete the circuit. At the beginning of the perfusion, the coronary network and the heart chambers are filled with blood. Blood clotting would block the coronary network. Therefore, at first, the infusion solution is not recycled in order to wash the heart. Once the solution is clear at the level of the box, the solution in the pool is cooled to 4 °C to be recycled in the perfusion circuit and maintain a constant level in the high container. To measure the heart perfusion, a flow meter was placed inside the tube inserted in the aorta about 5 cm above the aortic valve and a pressure sensor was placed at the level of the box containing the heart.

### Ultrafast ultrasound imaging of perfused hearts

To image the coronary arteries of the perfused heart, the ultrasound probe was positioned in contact with the box with a coupling gel. This probe was attached to a four-axis motor module with three translational degrees of freedom (VT-80 translation motors, PI) and one rotational degree of freedom (DT-80 rotary motor, PI). The positioning of the probe was controlled by a real-time B-mode to image long-axis or short-axis sections of the heart at different positions at the basal, middle, or apical level as shown in Fig. 2.

We used a linear probe (192 elements with a 0.2-mm width and 0.2-mm pitch, centered at 6.25 MHz) connected to a 256-channel ultrasound scanner (Vantage Verasonics, Kirkland, USA). An ultrafast imaging sequence consisting of 11 plane waves transmitted at angles of (–10; –8; –6; –4; –2; 0; 2; 4; 6; 8; 10°) at a PRF of 7.6 kHz was transmitted for 220 ms (to generate 150 images) and repeated 60 times for a total accumulation time of 13 s.

The signals received by the system were sampled at 25 MHz with corresponding 100% mode decimation. 2D delay and sum beamforming with coherent

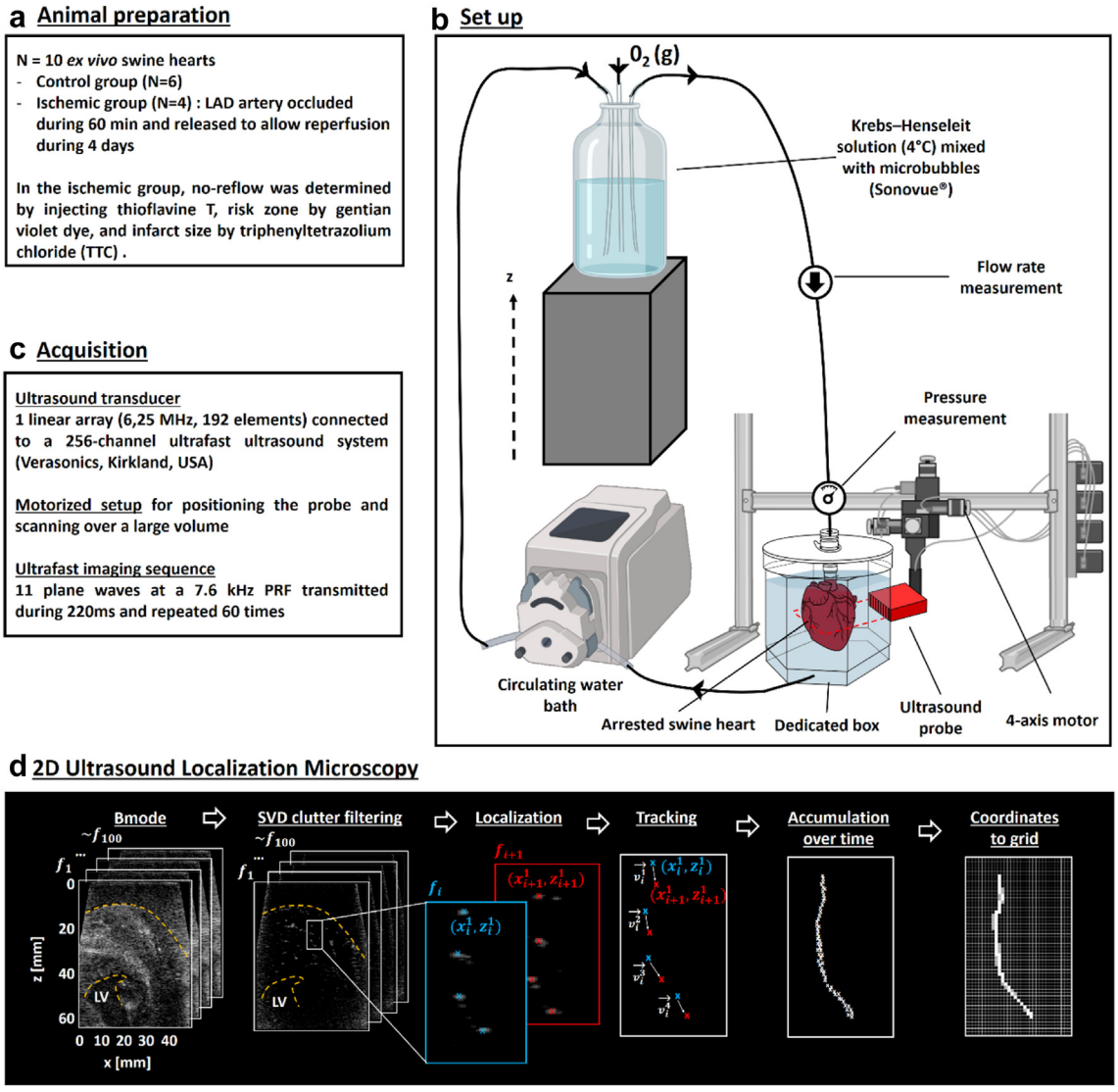


***Fig. 1:*** **Experimental setup.** a) Normal and infarcted swine hearts were studied *ex vivo*. b) Ultrasound Localization Microscopy imaging of the non-beating heart with a retrograde perfusion experimental setup (figure created with Biorender.com). c) An ultrafast imaging sequence was implemented for a linear probe. d) Principle of 2D Ultrasound Localization Microscopy (ULM).

compounding was performed to obtain in-phase and quadrature (IQ) demodulated the ultrasound images[13] at an effective imaging rate of 690 Hz. Images of 65 (depth) × 50 (lateral) $mm^2$ were reconstructed with a pixel size of 0.12 × 0.2 $mm^2$. Beamforming was implemented in CUDA language and performed on a GPU (NVIDIA GeForce RTX A6000). The IQ data were then filtered using the Singular Value Decomposition (SVD) approach for each block of 150 images[14] and removing the first 15 eigenvectors.

All processing was performed with MATLAB software (2020b, The MathWorks Inc., USA) using a 32-core AMD processor at 3 GHz. The processing time was approximately 5 min for beamforming and 4 min for SVD filtering plus Ultrasound Localization Microscopy processing, i.e., 9 min to obtain a super-resolved image of the coronary arteries at a given probe position.

Because the heart has larger dimensions (approximately 12 cm in length in the basal-apical direction and 10 cm in width in the minor axis) than the imaging field of view, a scan was performed in the basal-apical direction to scan the entire volume. The heart was also rotated at the level of the aorta so that the probe positioned on one of the 6 faces of the hexagonal box could image a complete cross-section of the heart.

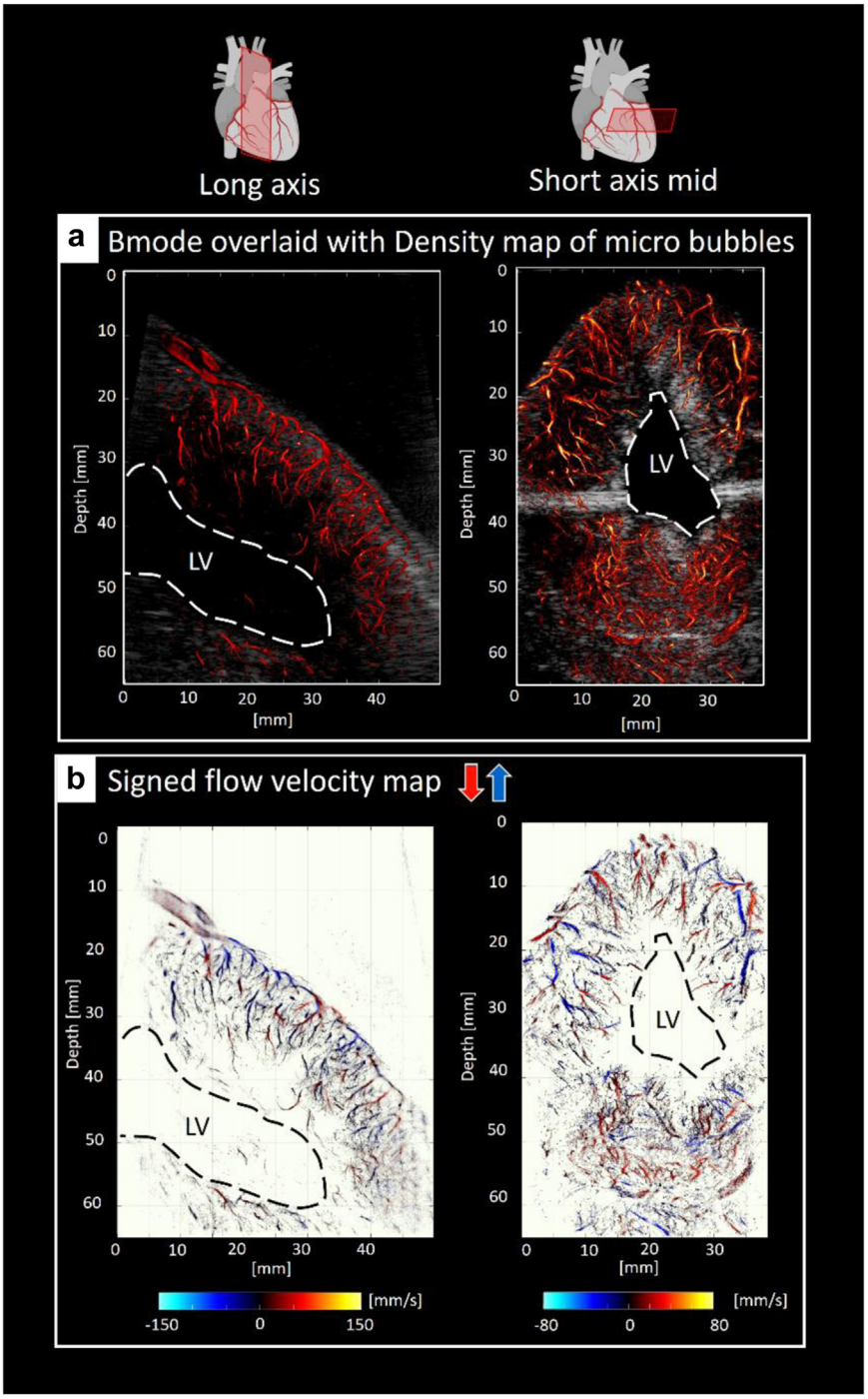


***Fig. 2:*** **2D ULM of the coronary vasculature of the ex vivo perfused control swine heart.** a) Density maps (number of MB) for long-axis and short-axis slices. A B-mode was overlaid to identify coronary anatomy within the heart tissue. b) Signed flow velocity (red: downward flow and blue: upward flow). On both panels, the left ventricle cavity was segmented manually and is depicted with a dashed line. LV = Left Ventricle.

### ULM processing

The ULM algorithm used was largely inspired by the one proposed by[15] and chosen for its computational speed (the computation is parallelized on CPU for the different image blocks). It has been slightly modified by taking some steps from the one described in[16] and is illustrated in Fig. 1d.

Once the IQ data were filtered to remove the tissue signal, the MB were detected as the local maxima in the image with a high correlation (>0.65) with a typical point spread function (PSF) (imaging response of an isolated MB, modeled as a Gaussian spot with axial and lateral dimension equal to the wavelength). Super-resolved localization of the pixel centers was then performed using a radial symmetry method inspired by.[17] Tracking of MB positions over time or tracking was performed using an implementation of the Kuhn-Munkres algorithm[18,19] or Hungarian method (https://github.com/tinevez/simpletracker, Jean-Yves Tinevez, 2021) with a maximum distance between 2 successive positions corresponding to a maximum speed of 400 mm $s^{-1}$. Only trajectories with MB detected in at least 10 successive images were selected. A Lagrangian approach was used to compute the MB velocity fields. The instantaneous velocity of each particle was thus calculated as the ratio between its displacement vector and its time sampling The obtained trajectories were used to calculate the components of the MB velocity vector (along the probe x-axis and the depth z-axis) as well as their absolute velocity. A linear spatial interpolation was added on each trajectory to count one MB detection in each pixel along its trajectory. Different maps were then reconstructed with isotropic pixels of 12.3 × 12.3 $\mu m^2$ (approximately $\lambda/20 \times \lambda/20$). MB density maps (number of MB) were calculated by counting all MB detected in a pixel during the acquisition time. Velocity maps were calculated as the average velocity of MB passing through that pixel. Finally, a signed velocity map was obtained by multiplying this average velocity by the sign of the velocity component along z.

## Motion correction

A 2D motion correction was used to compensate for small movements of the heart during the acquisition (swaying and slight swelling of the heart) even if the heart was non-beating. For each block, the unfiltered B-mode image (with tissue) averaged over a few hundred images were re-aligned with the first block of the acquisition taken as reference. The registration between the two images was computed using *imregtform* function in MATLAB using rigid transformations and the mean square error metric configuration. The resulting transformations were applied to the MB positions to obtain the realigned maps.

## Visualization and quantification

### *Reconstruction of large field of view*

The MB density, velocity, and signed velocity maps were overlaid on a B-mode image to be able to display coronary flows within the anatomy of the cardiac tissue. A complete short-axis slice of the heart was reconstructed by aligning images for each probe position on each of the 6 faces of the box. For each facet of the box, a transformation matrix with translations and rotations was deduced analytically from the hexagonal box geometry and applied. A registration was eventually done manually during post processing to correct small misalignments. In overlapped regions of the hexagon, the maximum value of MB density was selected.

### *Quantification of vessel diameter*

Quantification of vessel diameter was performed on the reconstructed density maps with isotropic pixels of 20 × 20 $\mu m^2$. In Amira software (Amira software v.6.0.1, Visualization Sciences Group, USA), a Gaussian filter was applied (sigma = 20 µm and 3 × 3 pixel kernel) as well as the "auto-skeleton" function, which, when the density value exceeded 1, segments the vessels and obtains the graph of the center of the detected vessels also called skeleton. The radius was then calculated for each point of the detected skeleton. To detect the smallest vessels, density maps were reconstructed with isotropic pixels of 12.3 × 12.3 $\mu m^2$ and the diameter was measured using Full Width at Half Maximum (FWHM).

### *Flow quantification*

Using velocity maps, flow velocities were measured as follows: the maximum velocity on the velocity profile from the section of a vessel was measured. An example is shown in (Supplementary Figure S1c). For NR hearts, super-resolved ultrasound imaging of the coronary arteries was compared with postmortem photographs of the left ventricle. In particular, areas of no-reflow, revealed under UV light with Thioflavin T, were quantified with ULM imaging. Microbubble perfusion was measured in two regions of interest: a non-ischemic area (outside the occluded coronary bed) and an NR area. Two parameters were measured to assess the perfusion flow: the number of tracked MB per $mm^2$ as well as the average velocity of these microbubbles on a larger grid with a pixel size of 3.8 × 3.8 $mm^2$ to detect the no-reflow areas. The American Heart Association (AHA) classification[20] was also used to identify areas normally perfused by the LAD artery.

## Control staining of no-reflow hearts

After the completion of the protocol of myocardial ischemia-reperfusion, (i.e., after 4 days of coronary artery reperfusion), the animals were re-anesthetized and a solution of Thioflavine T (2%) was administered intravenously to determine the areas with no-reflow (N = 2 pigs). Thioflavin T binds to the endothelium which provokes the fluorescence of the perfused tissue when exposed to ultraviolet light. The no-reflow areas appear dark by the absence of fluorescence. Then, the LAD was reoccluded at the same previous site and crystal violet solution (0.8%) was administered intravenously to delineate the previously occluded vascular bed (area at risk) (N = 3 pigs). In other words, the previously ischemic zone (i.e., areas of the heart not perfused for 60 min) was identified by the absence of a gentian violet

dye while the rest of the heart was stained (Supplementary Figure S2b). The heart was then excised for ultrasound imaging.

When ultrasound imaging of the coronary arteries was completed, each heart was removed from the *ex vivo* perfusion mount. The left ventricle was separated from the right ventricle and cut into 6 slices (short axis) from the apex to the base. Each slice was then incubated in a solution of triphenyltetrazolium chloride (1%, TTC) to delineate the infarct. Viable tissue appeared in red while the infarcted areas were identified as the white zones (Supplementary Figure S2a). Finally, the slices were placed under ultraviolet (UV) light and areas of no-reflow were identified by the absence of fluorescence in dark (Supplementary Figure S2c). Slices were then formalin-fixed and pictures were taken and compared to ULM images (Supplementary Figure S3).

### Response to perfusion pressure

Among the control group, a control experiment was performed on N = 3 hearts perfused at two pressure levels. The perfusion solution was first placed at a height of ~1.2 m from the heart giving a perfusion pressure of 87 mmHg. Then the solution was placed at a height of ~1.8 m with a perfusion pressure of 132 mmHg. The peristaltic pump allowed the solution to be refilled as the infusion progressed to maintain a constant level in the bottle and thus a constant pressure. The aortic perfusion rate was measured with a flow meter after calibration. For the N = 3 hearts, flow velocity as well as diameter were measured for 3 vessels of similar diameter (533 ± 165 μm). The means of these velocities per heart were then compared for the two perfusion pressures. Flow rates measured by the flow meter were also compared for the two perfusion pressures. Eventually, the ratio of the flow rate (flow rate at 182 mmHg/flow rate at 87 mmHg) was computed for each vessel knowing their diameter and flow velocity and averaged for each heart. This ratio was compared with the ratio of aortic perfusion flowrate measured by the flow meter and taken as control measurement.

### Ethics

The experiments were approved by the animal ethics committee [ComEth AFSSA-ENVA-UPEC agreement #29505] in compliance with the French regulations concerning the care and use of laboratory animals.

### Statistics

The averaged flow velocities measured in 3 vessels of similar diameter for the N = 3 hearts were compared for the two perfusion pressures using a paired, 1-tailed Student t test. Aortic flow rates measured by the flow meter were also compared for the two perfusion pressures using the same test. Eventually, the mean ratios of flow rate measured in 3 vessels of similar diameter for the N = 3 hearts were compared with the ratios of aortic flowrate using a two-tailed paired Student t test. For all box plots, the median (center line), first and third quartile (box), and values at 1.5 × interquartile range (IQR) (whiskers) were shown. All data points were plotted individually and paired data were linked by a line. A statistically significant test was inferred for $P < 0.05$ with: n.s: not significant, *: $P < 0.05$. Eventually, values were presented as mean ± standard deviation unless specified.

### Data availability

Data that support the findings of this study are available from the corresponding author upon reasonable request. Researchers wishing to obtain the raw data must contact the Office of Research Contracts at INSERM to initiate a discussion on the proposed data transfer or use.

### Role of funders

The funders had no role in study design, data collection, data analyses, interpretation, or writing of the manuscript. The corresponding author (C. Papadacci) had full access to all the data and the final responsibility for the decision to submit for publication.

## Results

### Flow anatomy of the coronary microcirculation

A box scan provides multiple slices of the heart and reveals the anatomy of the coronary arteries (Fig. 2a) as well as their flow velocity (Fig. 2b). In this way, we were able to image the coronary arteries and quantify their diameter and flow velocity ranging from ~25 μm for small arterioles to 1 mm for the largest arteries with corresponding flow velocities of 10–200 mm/s.

### Flow quantification

#### *Study of arterial and venous flows*

Downward and upward flows were segmented in a region of interest by taking into account the sign of the component along z direction (depth) (Fig. 3a). In this region, vessels with descending flow toward the ventricle corresponded mostly to arterial flow and inversely upward flows corresponded mostly to venous flow. The diameters of the vessels were also measured automatically by skeletonization (Fig. 3b). The distribution of MB velocity was shifted to higher values for downward flows than upward flows (Fig. 3c).

#### *Effect of perfusion pressure*

On the N = 3 control hearts used to assess the effect of perfusion pressure, an increase of perfusion flow was observed (Fig. 4c) when the perfusion pressure was increased from 87 mmHg (150 ± 44 mL/min, N = 3) to 132 mmHg (237 ± 55 mL/min, N = 3, $P < 0.05$). Flow velocity was measured in 3 vessels of similar diameter for the 3 hearts and increased from 31 ± 11 mm/s at

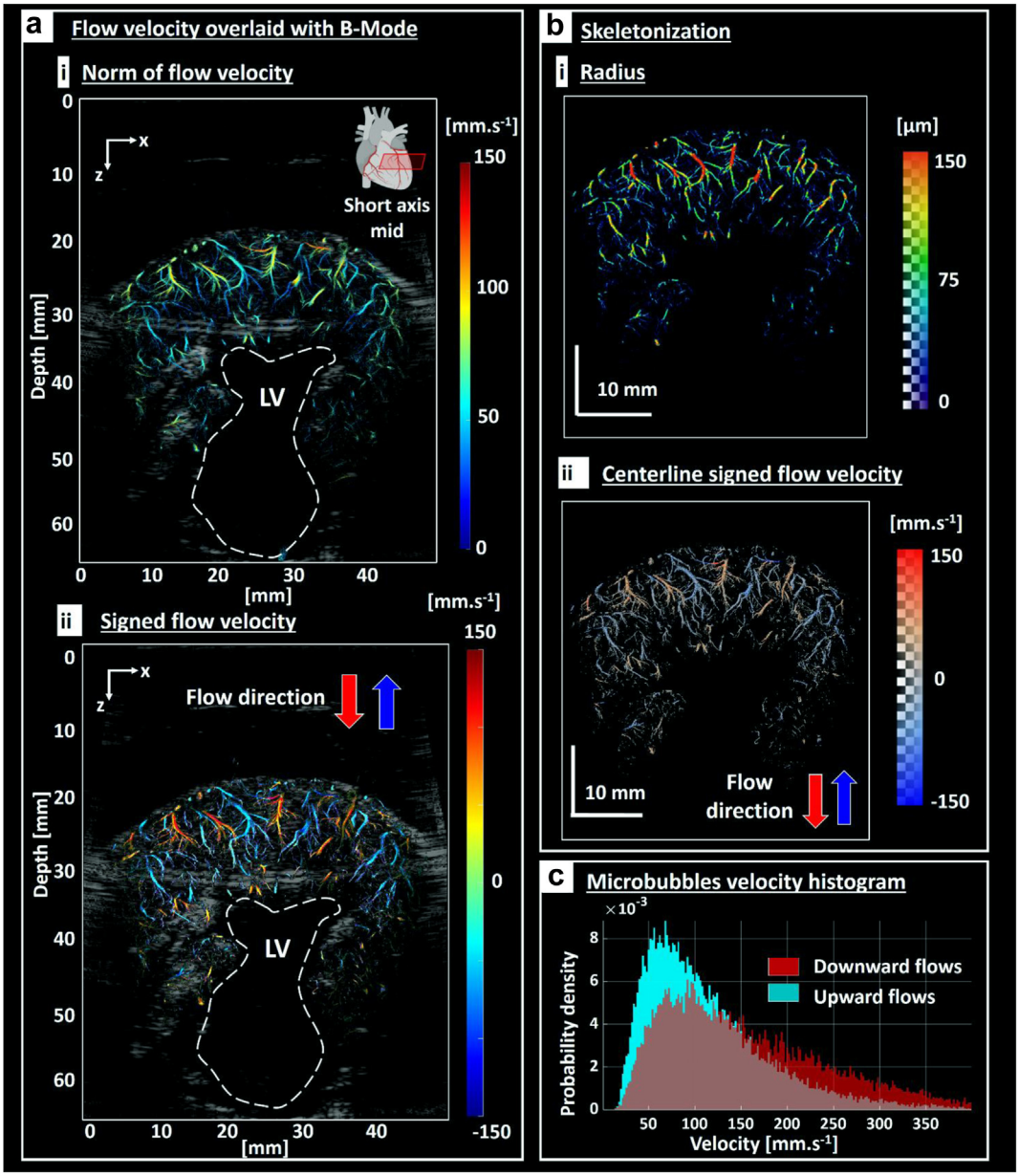


***Fig. 3*: Quantification of flow velocities for arteries and veins in a region of interest**. a) Flow velocity norm (i) and signed flow velocity (ii) (velocity norm multiplied by the velocity component along the depth z axis). b) Vessel diameters are measured automatically by skeletonization. Upward and downward flows are automatically segmented according to the sign of the velocity along z. c) MB velocity distribution is shifted to higher values for arteries downward flows which includes main arteries compared to upward flows including main veins.

87 mmHg to 47 ± 17 mm/s at 132 mmHg (N = 3, P < 0.05) (Fig. 4b). The increase in flowrate in these vessels (163% ± 44%, N = 3) was in good agreement with the increase in aortic perfusion flowrate (160% ± 22%, N = 3) measured by the flow meter and taken as a control measure (Fig. 4d).

*Perfusion in the no-reflow model*

Coronary microcirculation was compared on a whole short-axis section of the normal and NR hearts. In NR hearts, we detected areas of severely impaired micro-circulation (Fig. 5aii). These areas correspond to the areas of necrotic tissue (infarct zone) revealed by TTC

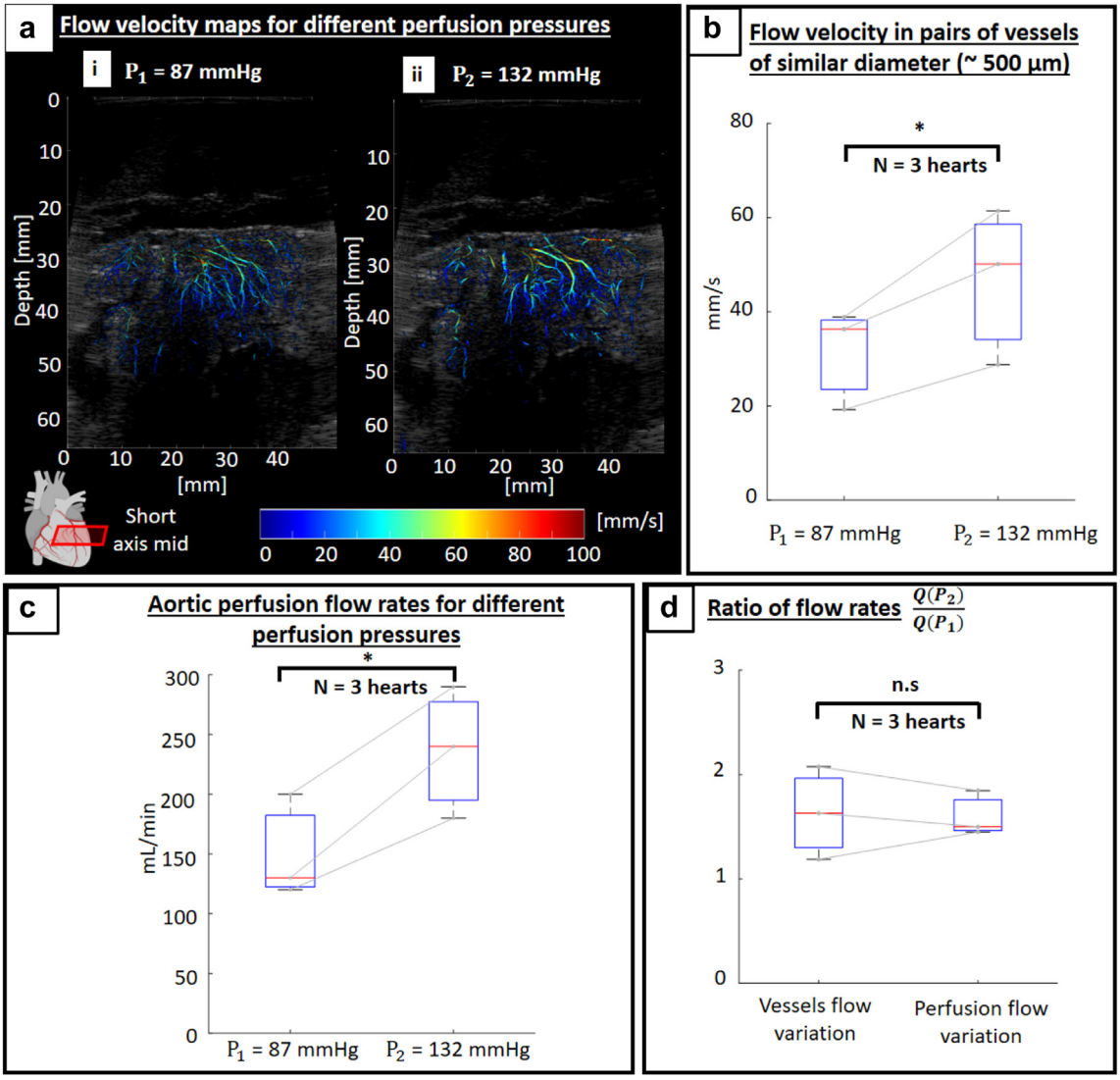


***Fig. 4:* Effect of perfusion pressure.** a) Velocity maps for perfusion pressure P1 = 87 mmHg and P2 = 132 mmHg. b) Flow velocity measured in 3 vessels of similar diameter for the 3 hearts. c) Aortic perfusion rates measured by a flow meter under both perfusion conditions. d) Ratio of flow rates measured in vessels by imaging is consistent with ratio of perfusion flow rates measured by the flow meter.

labeling (Fig. 5b). This area also corresponds to segments 7 and 8 of the AHA nomenclature, which are the segments of myocardium normally perfused by the LAD coronary artery.

As illustrated in Fig. 6b ii, an area of no-reflow (area with orange dotted line) was detected from two indicators proposed as measures of perfusion: the number of MB per unit area on a larger grid or the average velocity of these MB. This area corresponds to a zone of no-reflow revealed by the absence of fluorescence of Thioflavin T (area with orange dotted line in Fig. 6a). In this zone, the average perfusion is 204 ± 305 MB/mm$^2$ compared to an average perfusion of 3182 ± 1302 MB/mm$^2$ in the surrounding area (area with white line in Fig. 6bii). In this surrounding area, the microcirculation is reperfused as observed through ULM imaging or through the fluorescence of Thioflavin T.

A non-ischemic area which was outside the area downstream the occlusion was imaged as control (Fig. 6bi) with a homogenous perfusion.

## Motion correction

Although the heart is non-beating, small movements were observed (~1.5 mm over 5 min) due to rocking movements in the box, possible contractions, or the progressive swelling of the heart (edema). Block motion correction from the B-mode images of the tissue allowed better reconstruction of some vessels (Supplementary Figure S1).

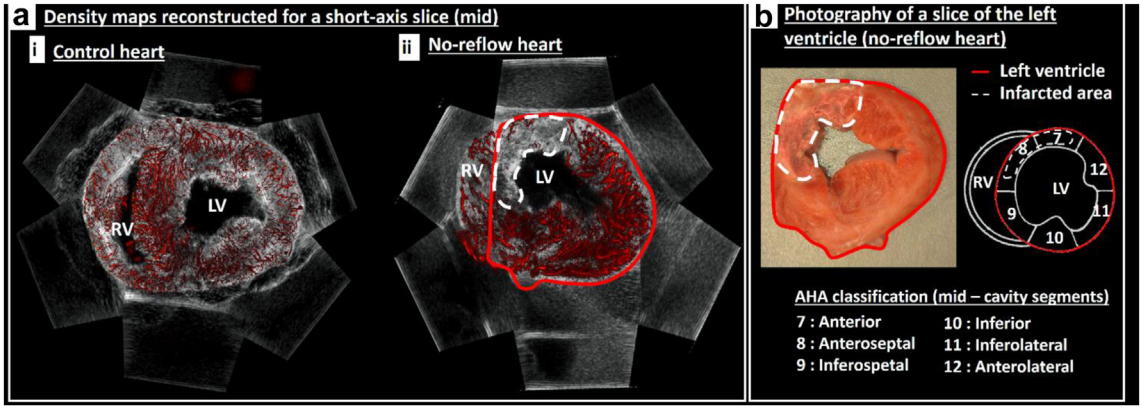


***Fig. 5:*** **Imaging of the coronary microcirculation for the control and no-reflow heart**. a) Density maps superimposed on B-mode images of cardiac tissue for the 6 sides of the box to reconstruct a complete view of a control heart (i) and a no-reflow heart (ii). The left ventricle is circled in red and the infarct area in white dotted lines. b) Photograph of a section of the left ventricle of the heart in (a.i) after TTC labeling. The necrotic area has a lighter color than the rest of the tissue that remained healthy. AHA nomenclature is given at the mid-level. The left ventricle and the infarct area are surrounded with the same color code. LV = Left ventricle RV = Right ventricle.

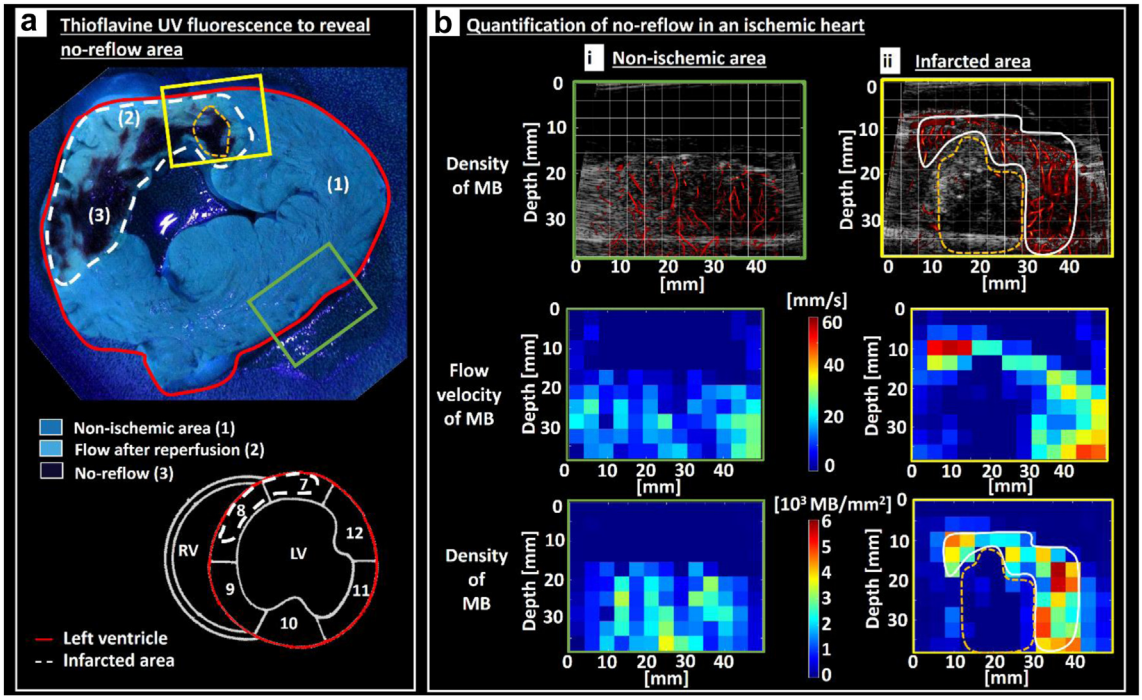


***Fig. 6:*** **Imaging the microcirculation to detect areas of no-reflow**. a) Photograph of a section of the left ventricle of a no-reflow heart under UV light revealing Thioflavin T fluorescence. The different areas: non-ischemic area (1), effectively reperfused area after release of occlusion (2), and no-reflow zone despite the release of occlusion (3) are captioned along with the AHA classification. The left ventricle is circled in red in the photograph and the AHA classification as well as the non-perfused zone during occlusion (in white dotted lines). b) Density maps (top panel) for a non-ischemic area (framed in green in i) and an area at risk (non-perfused during occlusion) (framed in yellow in ii). These two regions of interest are also shown in (a). In a grid (depicted in grey), average MB velocity (middle panel) and number of MB per unit area (lower panel) were computed. These two indicators allow quantification and detection of a no-reflow zone (orange dotted line) also visible by the absence of Thioflavin fluorescence. Perfusion is compared in a surrounding area (white line) where microcirculation was reperfused. LV = Left ventricle RV = Right ventricle.

## Discussion

In this study, we were able to image the coronary microcirculation of *ex vivo* swine hearts at a resolution of tens of microns (~25 μm). Tracking the trajectory of microbubbles over time allowed quantification of the flow velocity of the epicardial coronary arteries as well as in the microcirculation. Importantly, we detected and quantified altered perfusion of the microcirculation in reperfused hearts that underwent LAD occlusion, signing the well-known no-reflow phenomenon within the infarcted myocardium. Using average MB velocity and average density of MB per unit of surface as two ULM quantitative markers of perfusion, we detected these areas of coronary no-reflow in good agreement with a well-recognized anatomical pathology analysis under UV light and Thioflavin T labeling of cardiac tissue. Using other conventional blood flow imaging techniques such as power Doppler, no-flow regions with very little blood flow could be recognized as well. However, unlike ULM, power Doppler can quantify flow without imaging the coronary microcirculation anatomy. Thus, a big artery inside a no reflow zone would provide a large Power Doppler signal and mislead the diagnosis of a no-reflow zone without microcirculation reperfusion.

We studied a no-reflow model with 4 days of reperfusion. Lower or larger reperfusion durations could be used to investigate different clinical scenarios. Nevertheless, the no-reflow phenomenon has been demonstrated to increase up to 48 h[21] and then to remain stable between 2 days and 9 days.[22,23]

We proposed in this study a simple setup for the mapping of coronary microvascular flow on explanted perfused heart. Using a simple motorized device, a scan of the heart allowed the imaging of numerous short-axis views of the *ex vivo* heart at the basal, middle, or apical level or long-axis views. At a given position of the probe, the total time required to obtain a super-resolved image from acquisition to final image processing is 9 min including acquisition, writing to disk, beamforming and 2D ULM processing. This image covers a region of $65 \times 50$ mm$^2$ (depth and lateral directions respectively) and would allow to observe the microcirculation in a region of interest such as the anterior wall of the left ventricle for example. A complete short-axis section of the heart was obtained with a linear probe by scanning all 6 sides of the box and took 54 min. With an elevation width at the focal plane of approximately 0.7 mm for the linear probe, an exhaustive scan of the heart over 10 cm with a spatial step of 0.7 mm and on all 6 sides of the box would take over 128 h. A dedicated array with a larger field of view could be used to shorten this time as this probe would not require to go around the box, the field of view being sufficiently wide to cover the entire heart in short axis.

Better ULM images can be obtained as the acquisition time is slightly below the time needed to reach ULM saturation (Supplementary Figure S4). We could increase acquisition time to reach higher saturation at the cost of a longer heart scan time counting beamforming and processing in addition to acquisition time. Also, ULM vascular images should be interpreted carefully as there are several potential sources of spatial variation with depth including slide thickness and reconstruction algorithm. The slice thickness is indeed expected to vary with depth because of the ultrasound transducer focusing in elevation (in the direction orthogonal to the image). The performance of the algorithm to localize the microbubbles may be also depth-dependent. Adaptive localization algorithm with depth dependent point spread function could be implemented to solve this issue.

In the present study, we used an isolated retrograde perfused heart which represents a first major step in the long process of having a full operational transthoracic approach that could image the coronary circulation both in preclinical investigations and also at bedside in patients. In the long term, bringing this approach to clinics would require low frequency probes able to do 3D ultrafast imaging in a wide field of view, robust motion correction, ECG and breathing triggering and suitable clinical injection of MB. In the future, the availability of such transthoracic ultrasound approach would provide a highly valuable tool as compared to the noninvasive imaging methods, such as PET, MRI, X-ray computed tomography (CT), or other intravascular ultrasound approaches that require long acquisition time and do not provide immediate results. A bedside, reliable and widely available tool to diagnose no reflow is currently missing. The development of such a tool would enable an early identification of the no-reflow (i.e., in the cathlab) and the identification of patients who could benefit from a therapeutic intervention. This could help to identify patients to include in further studies on therapeutic agents. Other organs such as the kidney are frequently damaged by microvascular impairment with once again very limited interventions available. Studies recently demonstrated ULM imaging *in vivo* in humans[24,25] and with kidney allografts.[26]

Nevertheless, the isolated perfused heart is *per se* an interesting setup. It is commonly accepted as a preclinical setting in cardiovascular research in physiology, pathophysiology and drug developments and is widely used for the *ex vivo* investigation of ischemia-reperfusion injury. In particular, as it allows direct imaging of coronary no-reflow, it may provide valuable information for the understanding of no-reflow mechanisms and importantly, it would represent a valuable tool for the seek and the development of pharmacological strategies aimed at reducing the no-reflow phenomenon which is recognized today as an unmet need.[27] It should be emphasized that our approach device could also benefit to fundamental and translational research in other cardiovascular medical conditions that involve

coronary microvascular dysfunction. In fact, coronary microvascular disease is among the leading causes of heart disease. This is particularly the case with the growing issue of heart failure with preserved ejection fraction, diabetes, obesity but also arterial hypertension or with the hypertrophied heart. These situations would benefit from the direct imaging of the coronary tree and the quantification of coronary blood flow, both to evaluate the pathophysiological mechanisms and to investigate the effects of proposed pharmacological strategies. In the long term, this approach device could also be translated to clinical use in heart transplantation to characterize the viability of a cardiac graft. Graft quality assessment is critical to detect any potential damage induced by preservation and retrieval conditions. Currently, noninvasive evaluation of explanted heart grafts remains challenging and *ex situ* assessment relies mainly on qualitative interpretation by the surgeon based on the appearance of the organ, including anatomy, color, and manual palpation.[28] Finally, it should also be emphasized that the approach developed in the present study allows to access both functional, with the coronary blood flow, and anatomical information of the coronary circulation. This would allow to detect structural and vasomotor alterations that could develop in several cardiovascular disease.

Like any other imaging modality, it has limitations. The arrangement of the coronary network is complex and arbitrarily oriented in three dimensions, which limits the evaluation of ULM in 2D. Indeed, 2D velocity estimates may be underestimated when vessels are not perfectly aligned on the 2D slice. In addition, an important limitation of the method is the non-beating heart condition. For imaging the beating *ex vivo* heart, this system would not be suitable as large out-of-plane motion during the acquisition time would make the estimation and accumulation at a micrometer scale of the microbubble positions very difficult. A 3D ultrafast approach would thus be needed to estimate the contraction motion and correct it during the accumulation step as in.[8] In this previous study, coronary flow of *in vivo* and *ex vivo* rat beating hearts were imaged using 3D ultrafast imaging in diastole. Cardiac and breathing motion were successfully corrected. It should be noted that *in vivo* the coronaries are mainly perfused during the diastole which is significantly different than in *ex vivo* continuous perfusion. In humans, the selection of the diastolic phase (~500 ms) on the entire cardiac cycle (~1 s) is expected to increase the total acquisition time roughly by a factor of 2. *In vivo*, the presence of MB in the cavity may potentially shadow some deep parts of the myocardial wall. However, the localization and tracking process are not expected to be affected by microbubbles in the cavity as shown in[11] and.[29] However, this approach required an ultrasound scanner prototype with a high number of electronic channels which is costly, cumbersome and not adapted to clinical practice. Approaches to reduce the number of electronic channels such as Row-Column-Addressed probes (RCA) could be a promising tool for ULM *in vivo* as shown in.[30] The perfusion temperature used in this study is also a limitation as it may induce vasoconstriction.

For this application with a non-beating heart, scanning the heart with 2D ULM imaging is sufficient to map the coronary microcirculation slice per slice. As a control experiment, we studied the coronary perfusion of the heart under different perfusion regimes with physiological conditions of aortic pressure (at 87 and 132 mmHg). Note that the heart does not self-regulate under low temperature conditions. Also, this control experiment was performed only on N = 3 hearts and the statistical analysis should be carefully interpreted.

In conclusion, this study introduces a designed experimental setup and protocol to study the coronary microcirculation and no-reflow of an entire heart in a large animal preclinical model such as swine. As this approach device is rapid and simple, it opens new and interesting possibilities for the future pending further technological developments. It could represent a promising solution to study coronary perfusion and no-reflow in the reperfused heart at the acute phase of myocardial infarction. This approach has the potential to be extended to other clinical situations characterized by microvascular dysfunction.

#### Contributors

O.D, R.F, C.P, B.J and M.P did the concept and study design. O.D, P.M, P-M.C, A.B, J.D, L.S, R.G acquired data. O.D, A.B, C.P, B.J and M.P performed data processing. Writing and review of the manuscript: O.D, P.M, R.F, P-M.C, A.B, J.D, L.S, R.G, M.T, C.P, B.J, M.P. All authors reviewed and commented on the manuscript, and approved its final submission. Underlying data have been verified by C.P and M.P.

#### Data sharing statement

Data that support the findings of this study are available from the corresponding author upon reasonable request. Researchers wishing to obtain the raw data must contact the Office of Research Contracts at INSERM to initiate a discussion on the proposed data transfer or use.

#### Declaration of interests

All authors declare no competing interests.

#### Acknowledgements

This work was supported by Inserm research accelerator (Inserm ART) in Biomedical Ultrasound and by the French national research agency (ANR) under CORUS program (ANR-21-CE19-0002) and ANR-18-CE18-0015. The GPU RTX A6000 used in this work was awarded by the NVIDIA Academic Hardware Grant Program.

#### Appendix A. Supplementary data

Supplementary data related to this article can be found at https://doi.org/10.1016/j.ebiom.2023.104727.

#### References

1 Annibali G, Scrocca I, Aranzulla TC, Meliga E, Maiellaro F, Musumeci G. "No-reflow" phenomenon: a contemporary review. *J Clin Med*. 2022;11(8):2233.

2 de Waha S, Patel MR, Granger CB, et al. Relationship between microvascular obstruction and adverse events following primary percutaneous coronary intervention for ST-segment elevation

myocardial infarction: an individual patient data pooled analysis from seven randomized trials. *Eur Heart J*. 2017;38(47):3502–3510.
3 Gould KL, Johnson NP, Bateman TM, et al. Anatomic versus physiologic assessment of coronary artery disease. Role of coronary flow reserve, fractional flow reserve, and positron emission tomography imaging in revascularization decision-making. *J Am Coll Cardiol*. 2013;62(18):1639–1653.
4 Henningsson M, Shome J, Bratis K, Vieira MS, Nagel E, Botnar RM. Diagnostic performance of image navigated coronary CMR angiography in patients with coronary artery disease. *J Cardiovasc Magn Reson*. 2017;19(1):68.
5 Watanabe N, Akasaka T, Yamaura Y, et al. Noninvasive detection of total occlusion of the left anterior descending coronary artery with transthoracic Doppler echocardiography. *J Am Coll Cardiol*. 2001;38(5):1328–1332.
6 Fihn SD, Blankenship JC, Alexander KP, et al. 2014 ACC/AHA/AATS/PCNA/SCAI/STS focused update of the guideline for the diagnosis and management of patients with stable ischemic heart disease. *Circulation*. 2014;130(19):1749–1767.
7 Couture O, Hingot V, Heiles B, Muleki-Seya P, Tanter M. Ultrasound localization microscopy and super-resolution: a state of the art. *IEEE Trans Ultrason Ferroelectr Freq Control*. 2018;65(8):1304–1320.
8 Christensen-Jeffries K, Couture O, Dayton PA, et al. Super-resolution ultrasound imaging. *Ultrasound Med Biol*. 2020;46(4):865–891.
9 Foiret J, Zhang H, Ilovitsh T, Mahakian L, Tam S, Ferrara KW. Ultrasound localization microscopy to image and assess microvasculature in a rat kidney. *Sci Rep*. 2017;7(1):13662.
10 Cormier P, Porée J, Bourquin C, Provost J. Dynamic myocardial ultrasound localization angiography. *IEEE Trans Med Imaging*. 2021;40:3379–3388.
11 Demeulenaere O, Sandoval Z, Mateo P, et al. Coronary flow assessment using 3-dimensional ultrafast ultrasound localization microscopy. *JACC Cardiovasc Imaging*. 2022;15:1193.
12 Wang H, Ritter TA, Cao W, Shung KK. Passive materials for high-frequency ultrasound transducers [cited 2023 Jan 23]. In: *Medical imaging 1999: ultrasonic transducer engineering*. SPIE; 1999:35–42. Available from: https://www.spiedigitallibrary.org/conference-proceedings-of-spie/3664/0000/Passive-materials-for-high-frequency-ultrasound-transducers/10.1117/12.350684.full.
13 Szabo TL. *Diagnostic ultrasound imaging: inside out*. Academic Press; 2004:585.
14 Demene C, Deffieux T, Pernot M, et al. Spatiotemporal clutter filtering of ultrafast ultrasound data highly increases Doppler and fUltrasound sensitivity. *IEEE Trans Med Imaging*. 2015;34(11):2271–2285.
15 Heiles B, Chavignon A, Hingot V, Lopez P, Teston E, Couture O. Performance benchmarking of microbubble-localization algorithms for ultrasound localization microscopy. *Nat Biomed Eng*. 2022:1–12.
16 Renaudin N, Demené C, Dizeux A, Ialy-Radio N, Pezet S, Tanter M. Functional ultrasound localization microscopy reveals brain-wide neurovascular activity on a microscopic scale. *Nat Methods*. 2022;19(8):1004–1012.
17 Parthasarathy R. Rapid, accurate particle tracking by calculation of radial symmetry centers. *Nat Methods*. 2012;9(7):724–726.
18 Kuhn HW. The Hungarian method for the assignment problem. *Nav Res Logist Q*. 1955;2(1–2):83–97.
19 Munkres J. Algorithms for the assignment and transportation problems. *J Soc Ind Appl Math*. 1957;5(1):32–38.
20 Cerqueira MD, Weissman NJ, Dilsizian V, et al. Standardized myocardial segmentation and nomenclature for tomographic imaging of the heart. *Circulation*. 2002;105(4):539–542.
21 Rochitte CE, Lima JAC, Bluemke DA, et al. Magnitude and time course of microvascular obstruction and tissue injury after acute myocardial infarction. *Circulation*. 1998;98(10):1006–1014.
22 Wu KC, Kim RJ, Bluemke DA, et al. Quantification and time course of microvascular obstruction by contrast-enhanced echocardiography and magnetic resonance imaging following acute myocardial infarction and reperfusion. *J Am Coll Cardiol*. 1998;32(6):1756–1764.
23 Gerber BL, Rochitte CE, Melin JA, et al. Microvascular obstruction and left ventricular remodeling early after acute myocardial infarction [cited 2023 Jun 22]; Available from: *Circulation*. 2000;101:2734. https://www.ahajournals.org/doi/abs/10.1161/01.CIR.101.23.2734.
24 Huang C, Zhang W, Gong P, et al. Super-resolution ultrasound localization microscopy based on a high frame-rate clinical ultrasound scanner: an in-human feasibility study. *Phys Med Biol*. 2021;66(8):08NT01.
25 Denis L, Bodard S, Hingot V, et al. Sensing ultrasound localization microscopy for the visualization of glomeruli in living rats and humans [cited 2023 Jun 20] *eBioMedicine*. 2023;91:104578. Available from: https://www.thelancet.com/journals/ebiom/article/PIIS2352-3964(23)00143-3/fulltext.
26 Bodard S, Denis L, Hingot V, et al. Ultrasound localization microscopy of the human kidney allograft on a clinical ultrasound scanner. *Kidney Int*. 2023;103(5):930–935.
27 Hausenloy DJ, Chilian W, Crea F, et al. The coronary circulation in acute myocardial ischaemia/reperfusion injury: a target for cardioprotection. *Cardiovasc Res*. 2019;115(7):1143–1155.
28 López-Fraga M. *Guide to the quality and safety of organs for transplantation, 7th Edition, 2016*. 2016.
29 Goudot G, Jimenez A, Mohamedi N, et al. Assessment of Takayasu's arteritis activity by ultrasound localization microscopy. *eBioMedicine*. 2023;90:104502.
30 Jensen JA, Schou M, Jørgensen LT, et al. Anatomic and functional imaging using row-column arrays. *IEEE Trans Ultrason Ferroelectr Freq Control*. 2022;69:2722–2738.